A Print-planning Technique Using Edge-weights to Align Toolpaths to Vector Fields

J. W. McKee*, I. A. Rybak†, R. V. Gonzalez†, J. T. Green†

*Department of Aerospace and Mechanical Engineering, The University of Texas at El Paso, El Paso, TX 79968

†Department of Engineering Education and Leadership, The University of Texas at El Paso, El Paso, TX 79968

Abstract

Print-planning software can solve many challenges that limit the functionality of additively manufactured parts. Custom slicing software was developed to optimize toolpath alignment with input vector fields. The software converts slices of 3D models into graphs with edge-weights. Print move edge-weights were calculated using the difference in orientation between edges and local vectors while travel moves were assigned edge-weights exceeding the largest print move weight. A Hamiltonian path solver generated toolpaths that align well with the input vector fields by choosing paths that minimized the total weight of selected edges. As a demonstration, a part was printed with fused filament fabrication having extrusions aligned to brush strokes from reference artwork which included custom color assignment realized through use of an active-mixing hotend. Although conventional infill patterns can align well with simple vector fields, this technique provides automated print patterns which can follow both simple and complex vector fields.

Keywords: Fused Filament Fabrication, Toolpath, Vector Field, Path Planning, Traveling Salesman, Local Composition Control

Introduction

Many additive manufacturing technologies are toolpath dependent processes. Some notable examples which span a wide range of materials and scales include fused filament fabrication (FFF) [1], continuous fiber extrusion [2], directed energy deposition [3], extrusion bioprinting [4], and ceramic paste extrusion [5]. Fused filament fabrication is among the most common AM technologies in use today. Continuous fiber FFF is highly dependent on toolpath since the fiber must align with the work being applied to have an impact [6]. Directed energy deposition is used to generate cutting edge metal structures for demanding applications like rocket engines [7]. Extrusion bioprinting is being researched to produce artificial organs [8]. Ceramic paste extrusion is used for producing piezoelectric actuators and sensors [9]. Despite their incredible potential, these technologies are limited by the defects caused by travel moves and by properties heavily influenced by toolpath direction. Even printing methods like powder bed fusion require hatch patterns which are derived using methods similar to those which determine toolpaths. Despite the wide variety of benefits to numerous industries offered by these AM technologies, they are all subject to software-generated toolpaths.

Many methodologies for producing toolpaths follow algorithms which ensure infill of the part such as rectilinear, concentric and Hilbert curve, which are optimal only for simple shapes. More complex shapes introduce a large number of travel moves and therefore defects and prolonged print times. These techniques are not physics informed but are ubiquitous throughout slicing software used in AM. As AM expands its application for production of end-use parts [10], it becomes increasingly necessary to advance slicing algorithms to increase performance and meet the objectives specific to the application. A wide variety of objectives exist but many are driven by the physics of the manufacturing process and application of the end use part. Steuben et al. demonstrated one such technique including a slicer that uses finite element analysis to inform infill pattern and percentage dynamically throughout a part to increase the strength and stiffness of the print [11–14]. Notably, toolpaths can impact the manufacturing process altering thermal characteristics [15] and can have a direct impact on part performance.

Many slicers attempt to generate continuous toolpaths which can improve part performance [16], reduce defects and print time [17], and allow for continuous fiber printing which can greatly improve part strength in the fiber direction [18,19]. Optimization of continuous paths is difficult and can be computationally intensive, as many algorithms must compare every possible path to ensure that the optimal path has been selected. Depending on the complexity of a part a continuous path may be impossible, such as situations when there are layers with separate geometries making travel moves a necessity. The quantity of travel moves can be reduced within and between disconnected sections to improve print quality when possible [20,21]. One approach used for continuous pathing is a traveling salesmen problem (TSP) solving algorithm which connects a series of nodes to create a path [22].

Print-planning software can solve many challenges that limit the functionality of additively manufactured parts [11,23]. Many such parts have anisotropic characteristics dependent on toolpath direction [24,25]. Commercial software for toolpath planning has some tuning capabilities but generally cannot produce the complex paths necessary to achieve the performance and characteristics desired for advanced end-use applications. information on some print objectives can be embedded in a vector field. A common example of such a vector field is the stress profile measured from finite element analysis. Zhang et al. [26] aligned sections of linear raster patterns with the general direction of a principal stress field within a section and Chermain et al. [27] used a vector filed to influence the appearance of FFF printed parts. To advance AM capabilities by improving print planning, this study sought to develop custom slicing software to optimize path alignment to input vector fields allowing for automated generation of complex toolpaths. Toolpath alignment also has an impact on the appearance of final parts which was explored to imitate the style of paint brush strokes [27]. The objectives of this study are:

1. Develop methods for selecting toolpaths with increased alignment to a vector field.
2. Demonstrate printing with toolpaths aligned to a vector field derived from an image.
3. Characterize the increase in alignment as compared to parallel print paths.

Methods

Software was developed to assist in print planning operations emphasizing development of a method which generates a toolpath informed by an input vector field. The process is primarily

composed of operations for geometry import, meshing, applying weights, and path solving. These print planning operations were applied to conditions that do not allow travel moves in order to form continuous toolpaths. Examples of these methods were processed with a variety of geometries and target infill patterns as outlined in Table 1. This print planning method was then expanded to selectively integrate travel moves into the toolpath to increase alignment with the vector field. Travel moves are generally limited or avoided in FFF if possible as they introduce defects in a part, some of which are described by [28].

Table 1 – Print Planning Parameters

Label	Region/Source	Graph Type	Graph Spacing	Target Print Pattern	Output	Filament	Travel Moves
Circular-Continuous	Triangle/STL	Print	1x Extrusion Width	Spiral Vectors	D	-	No
Circular-Travel	Triangle/STL	Complete	1x Extrusion Width	Spiral Vectors	D	-	Yes
Prusa 90°	Rectangle/STL	-	-	90° Linear	D	-	No
Prusa 45°	Rectangle/STL	-	-	45° Linear	D	-	No
Painting-Translucent	Rectangle/Painting	Print	1x Extrusion Width	Painting Vectors	D & P	W, N	Yes
Painting-White	Rectangle/Painting	Print	1x Extrusion Width	Painting Vectors	D & P	W	Yes
Painting-Color	Rectangle/Painting	Print	1x Extrusion Width	Painting Vectors	D & P	C, M, Y	Yes
Painting-Split	Split-Rectangle/Painting	Print	1x Extrusion Width	Painting Vectors	D & P	C, M, Y	Yes
Painting-Tilted	Rectangle/Painting	Print	1x Extrusion Width	Painting Vectors	D	-	Yes
Painting-Coarse	Rectangle/Painting	Print	Coarse	Painting Vectors	D	-	Yes

Output
D: Digital Print Path
P: Printed Specimen

Filament
W: White PLA
N: Natural PLA (Clear)
C: Cyan PLA
M: Magenta PLA
Y: Yellow PLA

This technology was further explored for developing print operations to mimic some physical characteristics of paintings. Methods were devised to interpret images to provide a representative vector field. In concept, this vector field provides guidance for the print pattern which resembles the general orientation of brush strokes but is more explicitly characteristic of edges within an image. Print patterns were explored using one input image under a variety of constraints. Specimens were printed following these patterns providing a representation of these methods implemented through FFF. They further demonstrate the use case of these techniques to mimic the brush strokes of existing artwork through additive manufacturing.

Software Development

All new software developed in this study was programmed in Mathematica 14. Functions native to Mathematica assisted with visualization which is also useful for the user during fine tuning of print operations. In addition to basic software functions, Mathematica has native functions that support geometry import, meshing, graph conversion, weighted graphs, path solving, and image processing functions which simplified the development of the larger operations described below.

Geometry Import and Meshing

As with most print planning algorithms, the print geometry must be defined. This software supports the use of computer models that identify volumes by surfaces such as the stereolithography (STL) file, commonly used by slicing programs. This file defines regions by faces, edges, and vertices. Computer models were imported into the custom software made in Mathematica. The STL regions were used to define 2D regions at print layer heights. The work investigated in this study emphasizes toolpath selection within a single 2D region of a print geometry but can be extrapolated to form 3D structures in a layer-by-layer fashion. For each layer, the rectangular bounding boxes of the print region were populated with evenly spaced points, separated by the distance of one extrusion width. The points were converted to a Delaunay mesh of triangles, which was then used to define a mathematical graph with triangle vertices and edges as graph nodes and edges. Graph nodes outside the print geometry and less than half an extrusion width from the region boundary were removed to ensure that the resulting print was constrained to be within the desired print geometry. A graph-based path planning method was used in this work since toolpaths can be tailored through design criteria weights assigned to the graph edges [29]. The edges of the resulting graph represent the potential print moves which may be selected for the toolpath. Each set of nodes and edges per layer were labelled a print graph since they only contained potential print moves and included no potential travel moves.

A simplistic method for enabling travel moves from any node to any other node is to make the graph a complete graph, meaning that it contains every possible edge between all the nodes. The edges which were not contained in the print graph were identified by generating a complement graph. These edges were treated as potential travel moves. One advantage of this complete graph is that it will always contain a Hamiltonian path ensuring many potential solutions, but this type of graph can also be computationally taxing for path finding algorithms since the graph contains many more edges which yield many more potential solutions.

Adding Edge Weights from Vector Fields

Vector fields may be used to represent a wide variety of load conditions, characteristics, properties, or desired outcomes. Vectors at the graph nodes were assigned from input vector fields. A unit vector aligned with each edge on the print graph was calculated and used to assign weights to the edges equal to the magnitude of the corresponding cross product of the edge and vertex unit vectors**.** The edge weight was assigned using the vector from only one of the two nodes. Which specific node was used for the calculation was selected arbitrarily. One possible advancement to this technique would be the use of directed edges with weights assigned based on the node at the origin of the directed edge. The native path solving algorithm in Mathematica 14 does not support graphs with weighted directed edges.

Path Solving and Toolpath Generation

Graphs with edge-weights were used to guide toolpaths by selecting a sequence of edges which visit each node of the graph exactly once, known as a Hamiltonian path which is a form of TSP solver. By visiting each node, this method generates a toolpath that has no overlap in path and

theoretically has 100% infill. Using a function which selects a Hamiltonian path with minimum total edge-weights will also minimize the path segment weights. Since edge-weights assigned in this study were configured to decrease when the edge is aligned with the vector field, optimized paths within a print only graph should be continuous and align well with the vector field. Travel moves may be necessary on some print graphs, as they do not contain a Hamiltonian path, can be minimized by assigning large weights to their corresponding edges. Optimized paths using a complete graph may also yield a continuous graph depending on what Hamiltonian paths are possible and on what weights are applied to the potential travel moves as compared to the weights of the potential print moves.

The optimized Hamiltonian path of a graph with many nodes and edges is not easily determined. A brute force methodology for Hamiltonian path optimization identifies every possible path and compares them. Such a technique is often time prohibitive even with abundant computing power since each path is run in sequence. Methods for approaching the optimal result without requiring analysis of every possible path has been extensively researched [30–32].

Mathematica's Hamiltonian path solver has options for different performance goals supporting operations for time efficiency or increased optimization of the result. When determining toolpaths, the solver was set to a "Speed" performance goal which is a modified greedy Hamiltonian algorithm native to Mathematica which assured quick solve times allowing for rapid testing and tuning of process parameters. This function also has the ability to automatically modify graphs by adding edges when it cannot quickly find a Hamiltonian path. Additional functions were configured in the software to identify when the Hamiltonian path contains such edges which were then treated as travel moves. Complete graphs were used to determine toolpaths when travel moves could be beneficial and increased processing times were not inhibiting. When processing complete graphs, the solver does not generate new edges since all possible edges between nodes already exist which tend to greatly increase solve time. For this reason, the larger graphs in this study were processed as print graphs.

Convert to Printer Instructions

Print files were written in G-code which is necessary for operating the mixing printer used. The node coordinates along the path were used to calculate X and Y components of G1 commands. Extrusion commands for each print move were calculated using a flow multiplier and the length of the corresponding print segment assuming constant extrusion width and height throughout the print path. Since the prints were composed of a single layer, the Z component of the G1 commands were set to one layer thickness for all commands. When printing with dynamic filament mix ratios, the composition ratios were assigned for each node along the path using M165 mix commands following the methods described by [33]. A series of predefined start codes were added to home the printer, ensure assigned temperatures were reached and instruct how the printer should properly interpret extrude commands. Similar end code was also added to re-home, cool the hotend and bed and reset print specific parameters.

Vector Field Preparation

Two vector fields were generated for testing these path planning algorithms. Both sets of fields were selected to be complex in nature, including vectors orientated in all directions and being composed of discontinuous streamlines such that a single streamline does not cover the entirety of the region. A simply defined field was generated with vectors set to $\langle -y, x \rangle$ corresponding with coordinates $\{x, y\}$. The result is the concentric circular field shown in Figure 1. A triangular prism STL was pared with this field which resulted in a sufficiently complex yet predictable path for alignment to be gauged optically.

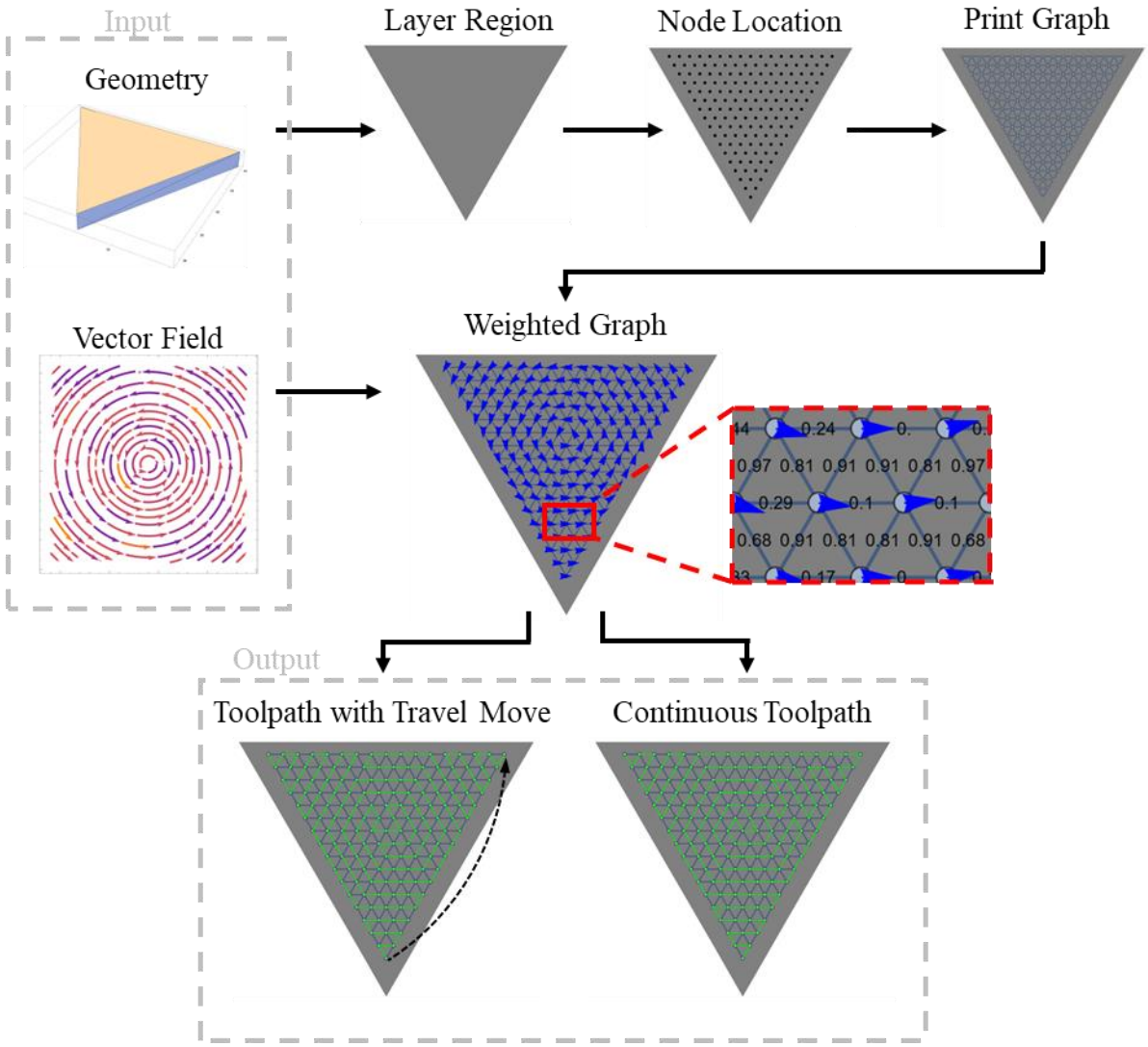

Figure 1 - Diagram of toolpath selection process for a triangular prism with a vector field corresponding with concentric circular streamlines. Process inputs include geometry and vector fields as well as process parameters. The geometry is sectioned into layers by region and nodes are positioned within the region. Each node is connected to neighboring nodes through graph edges which are assigned weights based on edge misalignment from the vector field. Two example toolpaths are shown with one continuous toolpath and one toolpath including a single travel move.

A second field was computed which aligned with the edges in an image of reference artwork. This painting was selected because the artist, Laura Dro, granted permission for it to be used in this study and because the edges with high Gaussian gradient intensity align well with the edge orientations contained in the default mesh. A scaled region was generated with an identical aspect ratio to the reference image. The region was scaled to fit within the print volume of the active mixing printer. The image was scaled to correlate relative pixel locations to graph vertex locations. Horizontal and vertical Gaussian derivatives were applied to a grayscale version of the scaled image and combined to compute the directional derivative along the edges which was converted to a discrete vector field as shown in Figure 2.

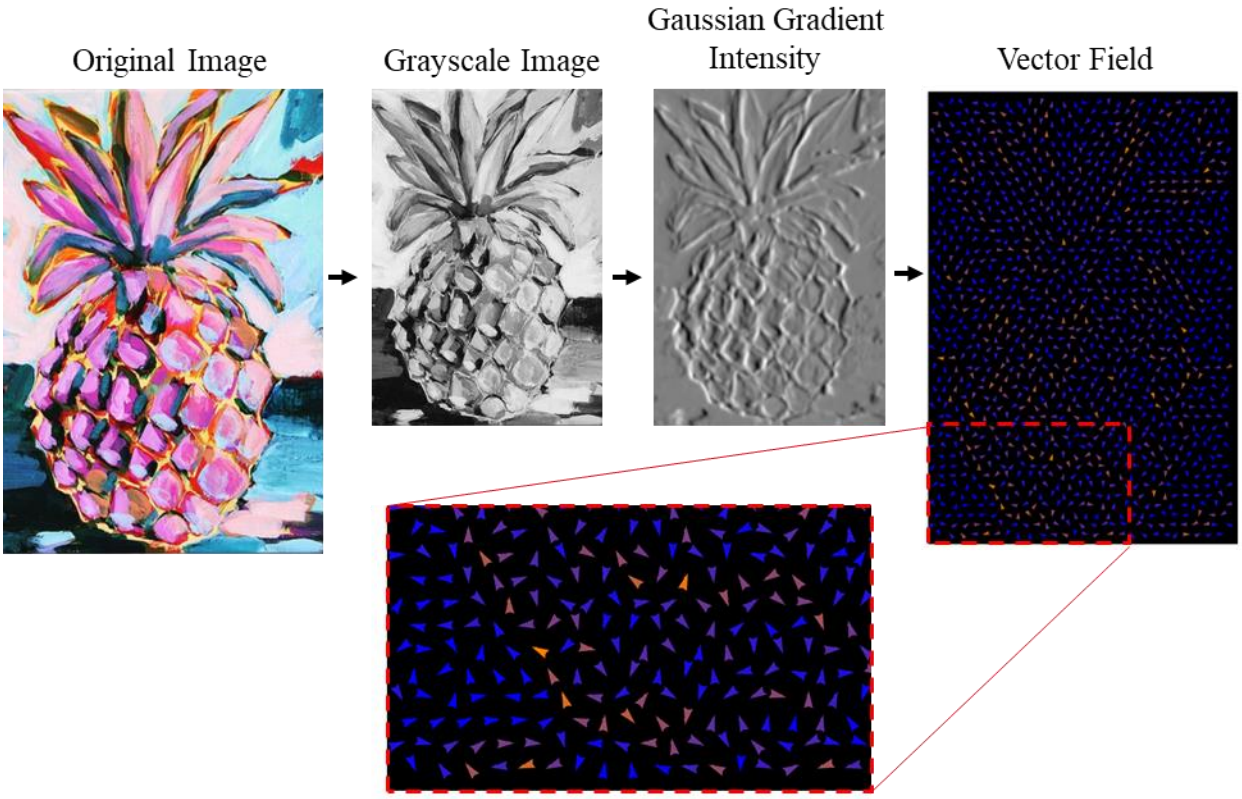

Figure 2 - Example of a vector field calculated from an image using Gaussian derivatives to solve the directional derivatives at each pixel which was then correlated with node locations. Vectors are scaled in color by vector magnitude with blue indicating low magnitude and orange indicating large magnitude.

Experiment Design

These combinations of vector fields and regions were used to demonstrate the ability of these algorithms to align a print path to a vector field even when using a relatively simple graph. An example of these processes applied to coarse graph are provided in Figure 3.

Only print graphs were used for the image aligned field, one with a simple mesh with horizontal triangle bases and one with all edges adjusted to improve overall alignment with the field. The Mathematica Hamiltonian with the “Speed” performance goal was used reducing solve time to under a minute using relatively inexpensive hardware even on graphs with over ten thousand nodes.

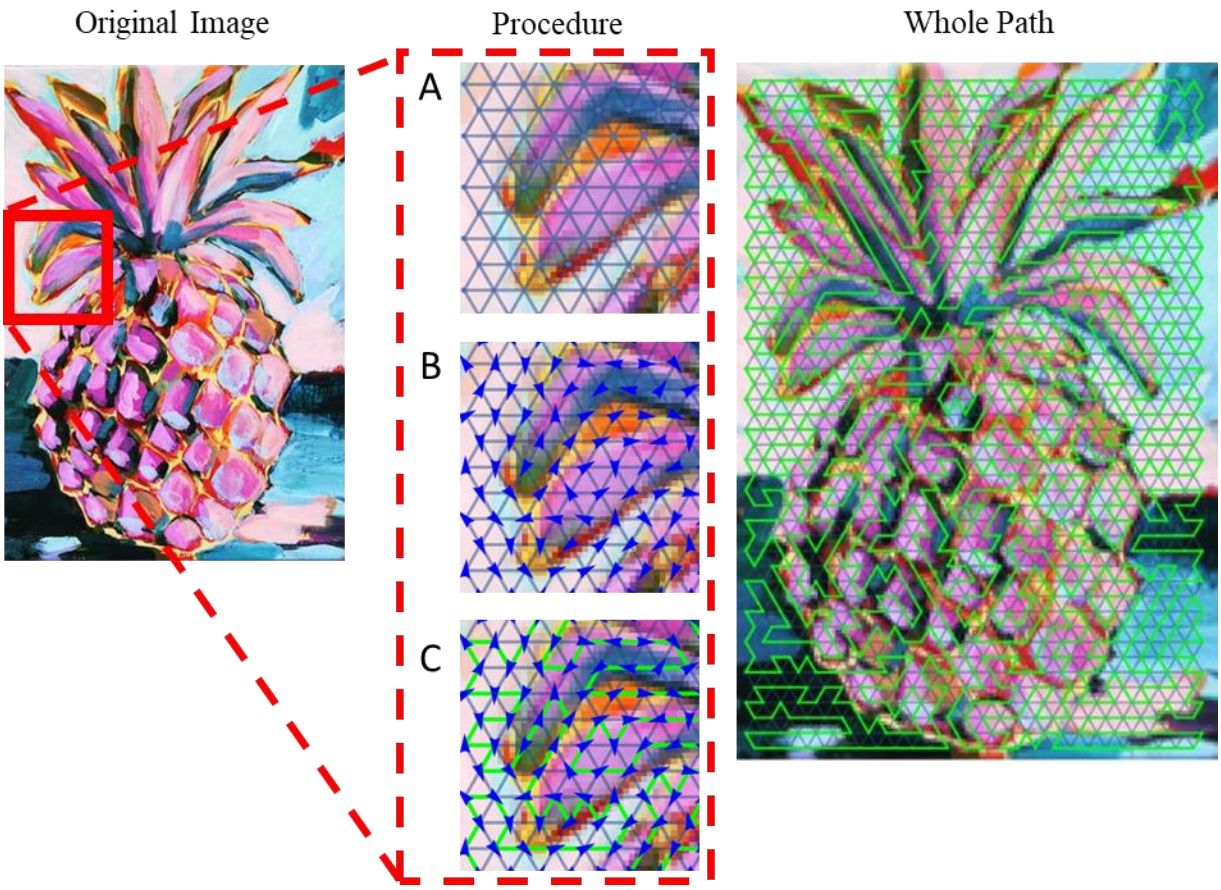

Figure 2 –Continuous toolpath developed from a source image. A) A coarse print graph has edge-weights informed by the B) vectors derived from the image at the node locations. The resulting C) continuous toolpath is shown in green which was selected to minimize edge-weights while connecting every node on the graph. Most toolpath segments align well with the vectors while deviation occurs as necessary to visit every graph node.

For a comparison to conventional linear patterns, a rectangular prism with dimensions and print parameters matching the regions for the previous tests was sliced in PrusaSlicer. 2.7.4 (Prusa Research a.s., Prague, Czech Republic) to generate a single layer. This was done twice with assigned rectilinear patterns at 45° and 90°.

Printing

For the painting informed paths, the image was converted to the cyan, magenta, yellow, and black (CMYK) color space and CMY pixel values at node locations were extracted. These proportions there converted to a ratio adding to one for the purpose of assigning mix commands at the nodes. A FFF active mixing hotend was used to print the calculated path allowing for proportional amounts of cyan, magenta and yellow polylactic acid (PLA) filaments to be blended corresponding to the calculated color values to try to achieve extrusion with color matching the reference artwork along the path. Increased volume flow rate of extrusion results in quicker color changes so a 0.8mm nozzle with prescribed layer height of 0.8mm was used The extrusion multiplier was set so that the nozzle would drag through previously extruded filament which is usually undesirable in FFF prints, but in this case, it highlighted the extrusion path, decreased voids

and helped to imitate the surface texture of some paintings. For these prints, white and natural PLA filaments were blended so that the resulting print could be overlayed on a screen displaying the reference image, in effect adding texture to the image. To demonstrate an increase in color accuracy, a second print toolpath was generated using two subregions of the reference image. The division of the regions was at the border between the pineapple and the background using image segmentation. The regions' toolpaths were solved individually, and the print instructions joined to show a difference in color between the regions.

Analysis

In addition to assessing toolpaths and print results qualitatively, calculations were performed to characterize these methods and the corresponding benefit for tailoring toolpath orientations. The alignment of a vector field to its corresponding graph and toolpath was quantified using the angle between the vectors at nodes to the orientation of the path segments and graph edges. As shown in Figure 3, the variable α is the angle between the vector at a node location as compared to the nearest print edge, and the variable β is the angle between a path segment and the vector at the corresponding node's location. The angle β was selected as an indicator for graph alignment since it represents the misalignment that persists even when the best print edge is selected. The mean α throughout a graph was used as an indicator for the overall alignment of a graph to its vector field, and the mean β of a toolpath was used as an indicator for the overall alignment of the path to the vector field. Other metrics which were used to quantify the toolpath include the average edge-weight throughout a toolpath, the total sum of edge-weights throughout a toolpath, and the proportion of path segments which are composed of best-aligned print edges. Toolpaths generated using conventional slicing software were analyzed by subdividing the toolpaths into segments approximately equal to one extrusion width with calculations for β referencing the vector at the starting location of each segment.

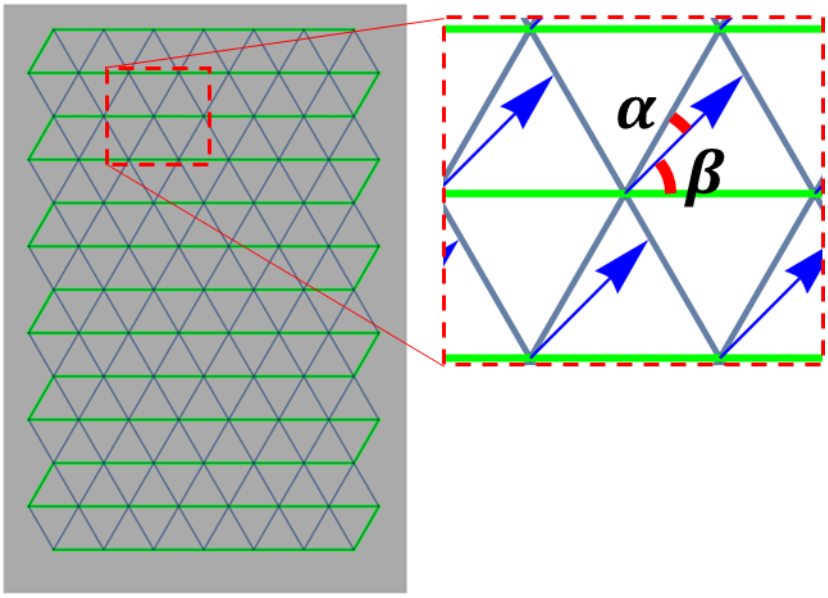

Figure 3 - Depiction of angles α and β on an example print graph within a rectangular region having the nodal vectors shown in blue and a toolpath shown in green. Note that α is the angle between the nodal vector and the nearest edge whereas β is the angle between the nodal vector and the corresponding path segment. In this example, α for this node is 15° and β for this node is 45°.

Results

The print paths which were generated using these methods generally follow their input vector fields with alignment quantified in Table 2. In Figure 1, the input vector fields pattern of concentric circles is evident for both the continuous and travel paths although alignment is improved in the path with the single travel move as seen in the top of the images. The inclusion of a travel move increased the alignment in this case which decreased the $\overline{|\beta|}$ value by 1.78° and increased the proportion of best aligned edges by 6.57% (Table 2). This increased alignment is also reflected in the reduction of the cost per volume of filament, from 0.1170 to 0.0937, and mean cost of the path which decreased by 0.00671 despite utilizing a travel edge with a higher cost than any print move. Other deviations in the paths stem from the sharp facets in the mesh and limited orientations of the available edges. $\overline{|\beta|}$ is calculated by looking at the alignment between the vector at each node along the path and the next segment of the path. Since edge weights only take into consideration the vector at the node on one end of the edge, the alignment represented by β may not be the alignment which contributed to the weight for that edge.

Table 2 - Toolpath performance metrics

Toolpath	$\bar{\alpha}$	$\overline{\lvert\beta\rvert}$	Path Segments matching Best Aligned Edges (%)	Mean Edge-weight along Path	Cost per Volume ($1/mm^3$)	Travel Move Count	Travel/Print x 10^3	Total Print Path Segments
Circular-Continuous	0.39°	20.51°	76.32	0.05615	0.1170	0	0	152
Circular-Travel	0.39°	18.73°	82.89	0.04944	0.0938	1	6.62	151
Prusa 90°	-	42.64°	-	-	-	0	0	13286
Prusa 45°	-	45.00°	-	-	-	0	0	13392
Painting-Rectangle	0.15°	28.70°	63.86	0.14	0.0967	16	1.16	13845
Painting-Tilted	0.02°	28.36°	64.27	0.14	0.0960	17	1.23	13808

The toolpaths computed from an input image of a painting demonstrate the ability of this methodology to generate a path regardless of the complexity of the target print orientations (Figure 3 and Figure 5). The image-derived vector fields tend to follow the edges of the features within the image (Figure 5 and Figure 6). Mathematica's path finding functions generated a path including non-print edges acting as travel moves with $\overline{|\beta|} = 28.70°$ and the best aligned edge, on average, misaligned by $\bar{\alpha} = 0.15°$. The rotated graph which was adjusted by 0.15° has an $\bar{\alpha} = 0.02°$, not 0° because the node locations shifted slightly resulting in a change of nodal vectors. Since the overall orientation of the default graph was already well aligned with the vector field, the tilted graph is only moderately improved by 0.13° and the difference between mean cost and cost per volume of extrusion are minimal. The custom toolpaths have greatly improved alignment when compared to 45° and 90° linear print patterns which have $\overline{|\beta|} = 46.73°$ and $\overline{|\beta|} = 42.68°$ respectively Table 2.

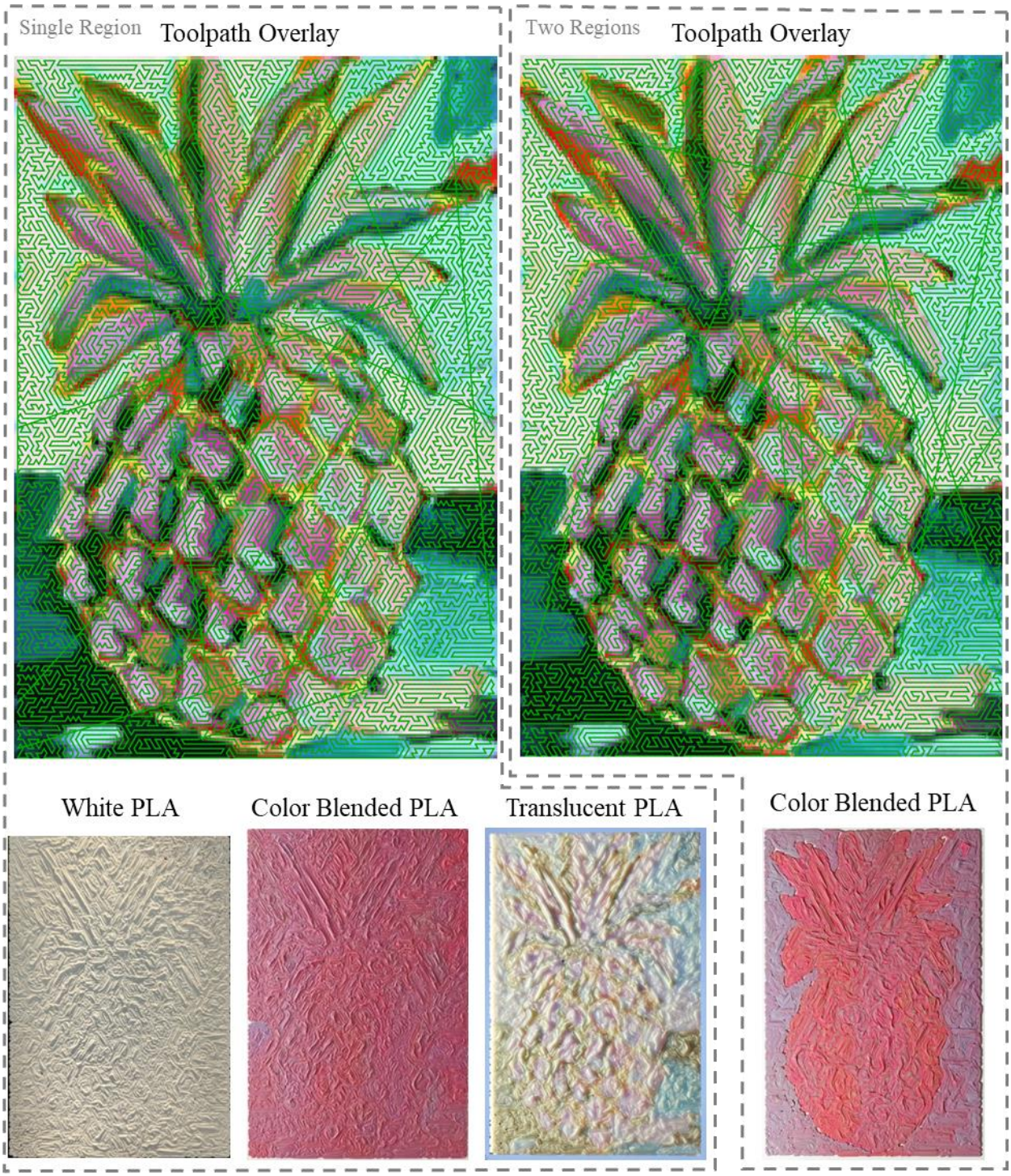

Figure 4 - Toolpaths and print results derived from a source image. The top images are the calculated toolpaths shown in green overlaying the source image. One toolpath (left) was generated using a single region matching the geometry of the source image. The other toolpath (right) was generated using two regions, one region matching the shape of the pineapple and another region for the rest of the image. Configuration for composition is indicated above the image of each print. The translucent print is positioned over a digital screen displaying the source image.

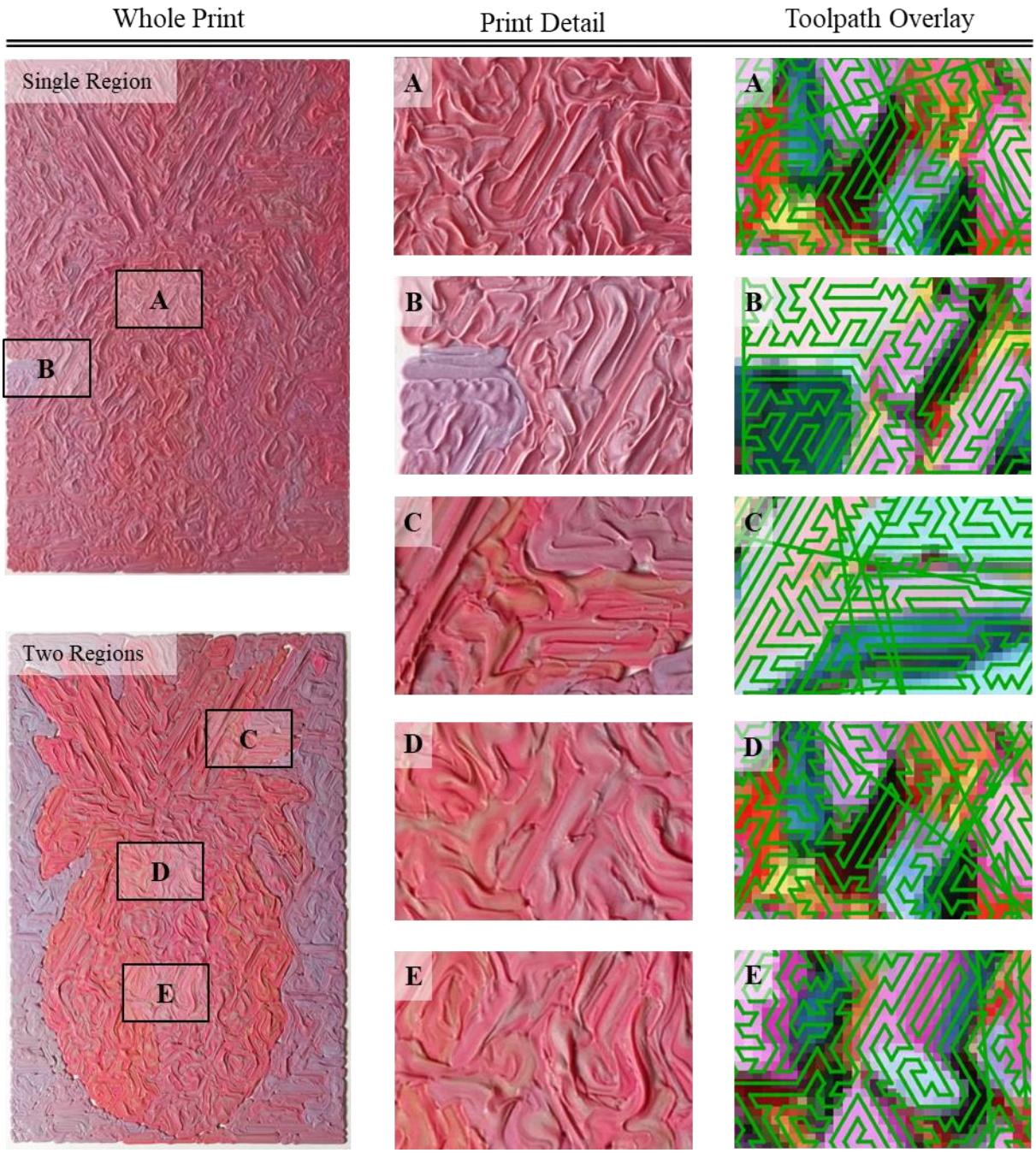

Figure 5 - Detail images of specimens printed with toolpaths informed by a source image. A variety of textures and print characteristics were observed including (A, B, D, and E) print patterns match the diamond shape on the pineapple's surface, (B) the horizon is visible within the print pattern, (C) texture is specific to the orientation of the leaves, and (E) a color shift is visible from the left to the right of the pineapple as is also observable in the original image.

Two image-based toolpaths are shown in Figure 5 overlaid on the scaled reference image with the resulting prints shown below. Specific details of the prints and paths are highlighted in Figure 6 which shows the paths alignment with certain features of the painting, some change in color that occurred and the resulting texture. In several cases the toolpath aligned very well with the edges in the painting making things like the horizon and shapes in the pineapple's skin visible even with the all-white print in Figure 5. The raised edges along extrusions give a painting like

depth to the prints which is a unique feature to using this path planning with FFF and lends itself well to these kinds of objectives. Some gaps exist between the two regions of the divided specimen because the meshes for these regions were generated separately and are shifted from one another. Despite following an identical mesh pattern this shift caused gaps larger than an extrusion width to be present at some locations near the interface between regions.

Discussion

The methods described are effective to generally align a toolpath to a given vector field which allows more accurate control of the path throughout a part than conventional print planning software. The flexibility of aligning to a vector field has broader applications than just artistic styling of printed part. This method could easily translate to the alignment of toolpaths with principal stresses calculated by finite element analysis to improve the strength of an additively manufactured part under those loading conditions. This capability combined with continuous pathing could be used for continuous fiber printing to further strengthen parts beyond what typical manufacturing processes can achieve which could further support additive manufacturing for end-use applications as compared to applications like prototyping.

Post processing of the toolpath could further help with alignment and eliminate gaps in the printed part as well as address other limitations in additive manufacturing such as the difficulty in printing sharp turns without over extruding. The relative simplicity of the meshes limited the best alignment possible, indicating that improved meshing algorithms may better align print paths to the vector field. One potential improvement may be possible by generating meshes with edges aligned to streamlines.

Discrete color accuracy was greatly limited by the rate of color change along the print path relative to the volume of the hotend's mix chamber. A larger print volume achieved through printer modification or division of the print into multiple larger segments could improve color accuracy. Allowing the mixing hotend to leave the build area and purge would also help achieve more accurate colors throughout a print and both methods should be explored in future work.

Conclusion

By using a Hamiltonian path solver that minimized the total weights of selected edges, toolpaths were generated that aligned well with input vector fields. As a demonstration, a part was printed with FFF having extrusions aligned to brush strokes from reference artwork which included custom color assignment realized through use of an active-mixing hotend. Although conventional infill patterns can align well with simple vector fields, this technique provides automated print patterns which can follow both simple and complex vector fields.

Acknowledgements

The authors wish to thank Hector Bocanegra Rodriguez for assisting in software development, Laura Dro for allowing her art to be used for this project, and to John Steuben who helped to lay the foundation for this project.

Funding

The authors wish to acknowledge the support from the UTEP Vice President of Student Affairs and Campus Office of Undergraduate Research Initiatives.

Conflict of Interest

The University of Texas System has a patent for technology described in this work for which Joshua T. Green is an inventor.

References

[1] A.R. Torrado, D.A. Roberson, Failure Analysis and Anisotropy Evaluation of 3D-Printed Tensile Test Specimens of Different Geometries and Print Raster Patterns, J. Fail. Anal. Prev. 16 (2016) 154–164. https://doi.org/10.1007/s11668-016-0067-4.

[2] S.M.F. Kabir, K. Mathur, A.F.M. Seyam, A critical review on 3D printed continuous fiber-reinforced composites: History, mechanism, materials and properties, Compos. Struct. 232 (2020) 111476. https://doi.org/10.1016/j.compstruct.2019.111476.

[3] K.S.B. Ribeiro, F.E. Mariani, R.T. Coelho, A Study of Different Deposition Strategies in Direct Energy Deposition (DED) Processes, Procedia Manuf. 48 (2020) 663–670. https://doi.org/10.1016/j.promfg.2020.05.158.

[4] Y.S. Zhang, G. Haghiashtiani, T. Hübscher, D.J. Kelly, J.M. Lee, M. Lutolf, M.C. McAlpine, W.Y. Yeong, M. Zenobi-Wong, J. Malda, 3D extrusion bioprinting, Nat. Rev. Methods Prim. 1 (2021). https://doi.org/10.1038/s43586-021-00073-8.

[5] W. Li, A. Ghazanfari, M.C. Leu, R.G. Landers, Extrusion-on-demand methods for high solids loading ceramic paste in freeform extrusion fabrication, Virtual Phys. Prototyp. 12 (2017) 193–205. https://doi.org/10.1080/17452759.2017.1312735.

[6] J. Naranjo-Lozada, H. Ahuett-Garza, P. Orta-Castañón, W.M.H. Verbeeten, D. Sáiz-González, Tensile properties and failure behavior of chopped and continuous carbon fiber composites produced by additive manufacturing, Addit. Manuf. 26 (2019) 227–241. https://doi.org/10.1016/j.addma.2018.12.020.

[7] N. Patel, S. Standbridge, M. Van Den Berghe, V. Devalaraju, Design and additive manufacturing considerations for liquid rocket engine development, AIAA Propuls. Energy Forum Expo. 2019. (2019) 1–43. https://doi.org/10.2514/6.2019-4392.

[8] E. Davoodi, E. Sarikhani, H. Montazerian, S. Ahadian, M. Costantini, W. Swieszkowski, S.M. Willerth, K. Walus, M. Mofidfar, E. Toyserkani, A. Khademhosseini, N. Ashammakhi, Extrusion and Microfluidic-Based Bioprinting to Fabricate Biomimetic Tissues and Organs, Adv. Mater. Technol. 5 (2020). https://doi.org/10.1002/admt.201901044.

[9] S.E. Hall, J.E. Regis, A. Renteria, L.A. Chavez, L. Delfin, S. Vargas, M.R. Haberman, D. Espalin, R. Wicker, Y. Lin, Paste extrusion 3D printing and characterization of lead zirconate titanate piezoelectric ceramics, Ceram. Int. 47 (2021) 22042–22048. https://doi.org/10.1016/j.ceramint.2021.04.224.

[10] V. Hassani, An investigation of additive manufacturing technologies for development of end-use components: A case study, Int. J. Press. Vessel. Pip. 187 (2020) 104171.

https://doi.org/10.1016/j.ijpvp.2020.104171.
[11] J.C. Steuben, A.P. Iliopoulos, J.G. Michopoulos, Implicit slicing for functionally tailored additive manufacturing, CAD Comput. Aided Des. 77 (2016) 107–119. https://doi.org/10.1016/j.cad.2016.04.003.
[12] J.M. Gardner, C.J. Stelter, E.A. Yashin, E.J. Siochi, High Temperature Thermoplastic Additive Manufacturing Using Low-Cost , Open- Source Hardware October 2016, (2018).
[13] L. Xia, S. Lin, G. Ma, Stress-based tool-path planning methodology for fused filament fabrication, Addit. Manuf. 32 (2020) 101020. https://doi.org/10.1016/j.addma.2019.101020.
[14] E. Sales, T.H. Kwok, Y. Chen, Function-aware slicing using principal stress line for toolpath planning in additive manufacturing, J. Manuf. Process. 64 (2021) 1420–1433. https://doi.org/10.1016/j.jmapro.2021.02.050.
[15] C. Zhang, C. Shen, X. Hua, F. Li, Y. Zhang, Y. Zhu, Influence of wire-arc additive manufacturing path planning strategy on the residual stress status in one single buildup layer, Int. J. Adv. Manuf. Technol. 111 (2020) 797–806. https://doi.org/10.1007/s00170-20-06178-w.
[16] X.A. Nguyen, P. King, A. Vargas-Uscategui, H. Lohr, C. Chu, A continuous toolpath strategy from offset contours for robotic additive manufacturing, J. Brazilian Soc. Mech. Sci. Eng. 45 (2023) 1–10. https://doi.org/10.1007/s40430-023-04544-9.
[17] B. Thompson, H.S. Yoon, Efficient Path Planning Algorithm for Additive Manufacturing Systems, IEEE Trans. Components, Packag. Manuf. Technol. 4 (2014) 1555–1563. https://doi.org/10.1109/TCPMT.2014.2338791.
[18] X. Chen, G. Fang, W.H. Liao, C.C.L. Wang, Field-Based Toolpath Generation for 3D Printing Continuous Fibre Reinforced Thermoplastic Composites, Addit. Manuf. 49 (2022). https://doi.org/10.1016/j.addma.2021.102470.
[19] W. Xu, H. Xu, Q. Li, P. Zhang, L. Yang, W. Wang, Stress-based continuous planar path planning for additive manufacturing, Adv. Eng. Softw. 188 (2024) 103544. https://doi.org/10.1016/j.advengsoft.2023.103544.
[20] C. Lu, W. Ma, S. Ba, D. Zhang, Resin content calculation of carbon fiber/poly (ether ether ketone) by thermogravimetric analysis, Polym. Test. 117 (2023) 107861. https://doi.org/10.1016/j.polymertesting.2022.107861.
[21] K.Y. Fok, N. Ganganath, C.T. Cheng, C.K. Tse, A 3D printing path optimizer based on Christofides algorithm, 2016 IEEE Int. Conf. Consum. Electron. ICCE-TW 2016. (2016) 1–2. https://doi.org/10.1109/ICCE-TW.2016.7520990.
[22] S. Singh, A. Singh, S. Kapil, M. Das, Utilization of a TSP solver for generating non-retractable, direction favouring toolpath for additive manufacturing, Addit. Manuf. 59 (2022) 103126. https://doi.org/10.1016/j.addma.2022.103126.
[23] M. Borish, A. Roschli, ORNL Slicer 2.0: Towards a New Slicing Paradigm Michael Borish*, Alex Roschli* *Manufacturing Demonstration Facility, Oak Ridge National Laboratory, Knoxville, TN 37932, (2021).
[24] N.S. Hmeidat, R.C. Pack, S.J. Talley, R.B. Moore, B.G. Compton, Mechanical anisotropy in polymer composites produced by material extrusion additive manufacturing, Addit. Manuf. 34 (2020) 101385. https://doi.org/10.1016/j.addma.2020.101385.
[25] D. Kokkinis, F. Bouville, A.R. Studart, 3D Printing of Materials with Tunable Failure via Bioinspired Mechanical Gradients, Adv. Mater. 30 (2018) 1–9. https://doi.org/10.1002/adma.201705808.

[26] H. Zhang, Y. Yao, Y. Ma, M. Lackner, Y. Jiang, A 3D printing tool-path generation strategy based on the partition of principal stress field for fused filament fabrication, Int. J. Adv. Manuf. Technol. 122 (2022) 1719–1735. https://doi.org/10.1007/s00170-022-09957-9.
[27] X. Chermain, C. Zanni, J. Martínez, P.A. Hugron, S. Lefebvre, Orientable Dense Cyclic Infill for Anisotropic Appearance Fabrication, ACM Trans. Graph. 42 (2023). https://doi.org/10.1145/3592412.
[28] J. Hergel, S. Lefebvre, Clean color: Improving multi-filament 3D prints, Comput. Graph. Forum. 33 (2014) 469–478. https://doi.org/10.1111/cgf.12318.
[29] G. Zhang, Y. Wang, J. He, Y. Xiong, A graph-based path planning method for additive manufacturing of continuous fiber-reinforced planar thin-walled cellular structures, Rapid Prototyp. J. 29 (2023) 344–353. https://doi.org/10.1108/RPJ-01-2022-0027.
[30] Y. Wang, The hybrid genetic algorithm with two local optimization strategies for traveling salesman problem, Comput. Ind. Eng. 70 (2014) 124–133. https://doi.org/10.1016/j.cie.2014.01.015.
[31] K. Singh, S.K. Bedi, P. Gaur, Identification of the most efficient algorithm to find hamiltonian path in practical conditions, in: Proc. Conflu. 2020 - 10th Int. Conf. Cloud Comput. Data Sci. Eng., 2020: pp. 38–44. https://doi.org/10.1109/Confluence47617.2020.9058283.
[32] N. Ascheuer, Hamiltonian path problems in the on-line optimization of flexible manufacturing systems, 3 (1995) 221.
[33] J.T. Green, I.A. Rybak, J.J. Slager, M. Lopez, Z. Chanoi, C.M. Stewart, R. V Gonzalez, Local composition control using an active-mixing hotend in fused filament fabrication, Addit. Manuf. Lett. 7 (2023) 100177. https://doi.org/10.1016/j.addlet.2023.100177.